



HAL
open science

Multi-Frequency TR-MUSIC Processing to Locate Soft Faults in Cables Subject to Noise

Moussa Kafal, Andréa Cozza

► **To cite this version:**

Moussa Kafal, Andréa Cozza. Multi-Frequency TR-MUSIC Processing to Locate Soft Faults in Cables Subject to Noise. *IEEE Transactions on Instrumentation and Measurement*, 2020, 69 (2), pp.1-8. 10.1109/TIM.2019.2896369 . hal-01982747

HAL Id: hal-01982747

<https://centralesupelec.hal.science/hal-01982747v1>

Submitted on 15 Jan 2019

HAL is a multi-disciplinary open access archive for the deposit and dissemination of scientific research documents, whether they are published or not. The documents may come from teaching and research institutions in France or abroad, or from public or private research centers.

L'archive ouverte pluridisciplinaire **HAL**, est destinée au dépôt et à la diffusion de documents scientifiques de niveau recherche, publiés ou non, émanant des établissements d'enseignement et de recherche français ou étrangers, des laboratoires publics ou privés.

Multi-Frequency TR-MUSIC Processing to Locate Soft Faults in Cables Subject to Noise

Moussa Kafal, *Member, IEEE* Andrea Cozza, *Senior Member, IEEE*

Abstract—Time-Reversal multiple signal classification (TR-MUSIC) has recently been shown to be an effective technique to locate multiple soft faults in wire networks, thanks to its sub-millimeter location accuracy. TR-MUSIC processes transmission and reflection data measured at a single frequency into a function of space, the pseudo spectrum, expected to present singularities only at a fault position. At frequencies high enough, the spatial periodicity that comes with the propagation of harmonic signals leads to multiples such singularities, of which only one represents the fault position, while the remaining are ghosts faults. TR-MUSIC was therefore introduced using a single continuous-wave excitation at frequencies low enough to avoid ghosts, an approach suitable only to noiseless configurations. This paper explores the effects of noise on TR-MUSIC fault location by first highlighting its high sensitivity to noise at low frequency. A potentially lower sensitivity is shown to exist at high frequencies, where ghost positions are found. A multi-frequency processing is introduced, allowing at the same time to solve the ambiguity in the fault position and to effectively control the impact of noise on its location accuracy. The proposed processing is shown to reinstate precise super-resolved estimates of fault locations even for signal-to-noise ratios as low as 5 dB, without requiring to the use of wide-band signals.

Index Terms—Fault detection, fault location, soft faults, complex wire networks, additive noise.

I. INTRODUCTION

CABLES in industrial settings are often exposed to potentially harsh conditions, which may lead to the appearance of either hard faults (open or short circuits), or soft faults, which are usually minor alterations (e.g., chafing) that affect a cable without impeding its nominal functions. Notably, the latter kind of faults have earned attention [1]–[7] as their evolution could be continuously monitored, in order to ideally intervene before their developing into hard faults, thus avoiding a sudden system collapse.

While most techniques rely on the use of wide-band excitation signals [3], [8]–[15], it has recently been demonstrated [16] that soft faults can be located by using single-frequency continuous-wave tests, and still obtain sub-millimeter precision, thanks to the super-resolution properties of time reversal-based multiple signal classification (TR-MUSIC) [17]. In particular, test signals below 10 MHz were shown in [16] to result in estimates of fault locations within a few millimeters, i.e., about 1/20000 of wavelength of the test signal. Similar spatial

resolutions would require test signals covering bandwidths spanning several GHz when using reflectometry techniques.

Theory has it that MUSIC-based processing can potentially achieve unlimited resolution with noiseless data. But real-life NUTs and the associated testing equipment are routinely affected by background noise, or signals during online tests, which might be sufficiently high to degrade the quality of MUSIC processing. In investigations on open-media applications of TR-MUSIC, [18], [19] have proven that in presence of noise the super-resolution expected from TR-MUSIC processing can not be reliably ensured.

This paper explores the impact of noise on the precision of fault location estimated with TR-MUSIC, proving that the previously introduced choice of using single-frequency processing at very low frequency is only suitable for negligible noise levels. Experimental results show that TR-MUSIC sensitivity to noise is inversely proportional to the frequency, suggesting that the ghost region, even though affected by ambiguity about the actual fault position, holds the potential for noise-robust TR-MUSIC fault location. The proposed solution is based on a multi-frequency processing that allows at the same time to solve the spatial ambiguity caused by the presence of ghost positions, while giving access to a larger pool of single-frequency estimators less affected by noise. The resulting processing is expected to be more suitable for practical configurations, where noise could potentially be sufficient to invalidate the low-frequency approach previously introduced.

The paper's structure is as follows: the basic aspects of TR-MUSIC processing applied to locating soft faults in a cable network are reviewed in Sec. II, while Sec. III presents an empirical analysis of the impact of noise on the resolution of TR-MUSIC for two topologies of networks under test (NUT). The high sensitivity of low-frequency data to noise is confirmed even for relatively good signal-to-noise ratios (SNR), e.g., 15 dB. The multiple-frequency approach is introduced in Sec. IV, exploiting the intrinsic coherence of fault-position estimates computed across different frequencies with TR-MUSIC. Design rules are derived enabling a robust implementation, depending on the required level of precision, in particular based on the number of tests required and the bandwidth over which the NUT is tested. Experimental results in Sec. V prove that this multi-frequency implementation can still ensure a millimetric resolution even when dealing with SNRs as low as 5 dB. Although in this case tests may need to be carried out at higher frequencies, the spatial resolution is shown to still be much higher than that achievable by reflectometry techniques.

M. Kafal is with the Laboratory of Reliability and Integration Sensors (LFIC) at the French Alternative Energies and Atomic Energy Commission (CEA)

A. Cozza is with the Group of Electrical Engineering - Paris (GeePs), CentraleSupélec, Univ. Paris-Sud, Université Paris-Saclay, Sorbonne Universités, UPMC Univ Paris 06, 3 & 11 rue Joliot-Curie, Plateau de Moulon 91192 Gif-sur-Yvette CEDEX, France Contact e-mail: andrea.cozza@ieee.org

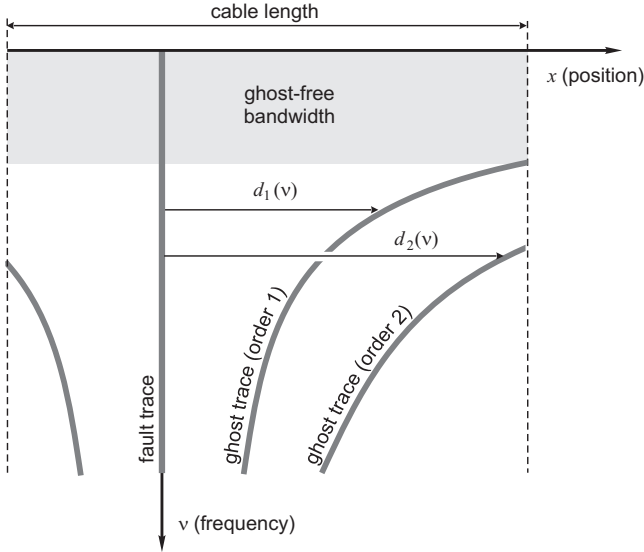


Fig. 1: Typical structure of the pseudo spectrum $\Phi(x, \nu)$ generated by TR-MUSIC for a cable, as the locus of points over the frequency-position plane where the pseudo-spectrum presents singularities.

II. TR-MUSIC FOR FAULT LOCATION

The basic operations involved in the use of TR-MUSIC technique in fault location, are here recalled; the interested Reader should refer to [16] for more details. All quantities in the following are functions of the frequency ν ; it might be dropped for the sake of brevity.

TR-MUSIC processing is intrinsically defined as a multi-static approach and relies on the availability of an NUT scattering matrix $\mathbf{S}_f(\nu)$, measured over N testing ports, e.g., by means of a vector network analyzer (VNA). It also requires baselining information, i.e., the reference response $\mathbf{S}_h(\nu)$ of a healthy version of the network [20], [21], which is fundamental step in any diagnostic technique for the case of soft faults. TR-based methods operate on the difference system $\mathbf{S} = \mathbf{S}_f - \mathbf{S}_h$, which can be shown to result in an equivalent description where a fault acts as a secondary source [22]. It also increases the maximum number M of faults that TR-MUSIC can detect, by removing the echoes generated by impedance discontinuities like junctions in an NUT.

The TR operator is the key behind most TR applications and is obtained from the difference scattering matrix \mathbf{S} as $\mathbf{K} = \mathbf{S}^\dagger \mathbf{S}$, where the superscript \dagger is the Hermitian transpose. TR-MUSIC can locate up to M faults, under the condition that $N > M$. In particular, the eigenvalue expansion of \mathbf{K} forms the basis of the TR-MUSIC method by identifying the noise subspace \mathcal{N} of \mathbf{K} . \mathcal{N} is formed by the eigenvectors deemed to have negligible eigenvalues, i.e., $\mathcal{N} = \text{span}\{\mathbf{u}_i : \lambda_i < \lambda_{th}\}$, with λ_i and \mathbf{u}_i being the eigenvalues and their corresponding eigenvectors, respectively; λ_{th} is usually set after analyzing the scree plot of the eigenvalues of \mathbf{K} .

The number M of faults is then given by the rank of \mathbf{K} , while their positions are inferred from local maxima in the pseudo-spectrum $\Phi(x, \nu)$, defined as [23]:

$$\Phi(x, \nu) = \left(\sum_{\mathbf{u}_i \in \mathcal{N}} |\mathbf{u}_i^\dagger(\nu) \mathbf{g}(x, \nu)|^2 \right)^{-1}, \quad (1)$$

with $\mathbf{g}(x, \nu) = [g_1(x, \nu), \dots, g_N(x, \nu)]^T$ a vector consisting of the N Green functions of the healthy NUT, which are defined as the N spatial distributions, in the coordinate x , of voltages observed along the NUT, when separately excited from each testing port. These distributions can be estimated from a numerical model of the NUT, e.g., based on transmission-line theory.

The typical structure of $\Phi(x, \nu)$ is shown in Fig. 1. The multiple traces are the loci of the peaks of the pseudo-spectrum, generated by the multiple peaks observed at each testing frequency. The fault position p is marked by a vertical trace, or fault trace, which is unique in its frequency invariance. Curved traces, or ghost traces, are caused by the periodicity of Green functions for harmonic signals propagating along transmission lines, appearing in (1). These traces can be identified by their coordinates $p_n(\nu)$, where $n \in \mathbb{Z}$ is their order, with $n = 0$ the fault trace. Transmission-line theory implies that (1) has a periodicity of half a wavelength, with ghost traces thus found at a distance

$$d_n(\nu) = p_n(\nu) - p = \frac{n\nu}{2\nu}, \quad (2)$$

with v the propagation speed along the cables.

As opposed to open-media applications of TR-MUSIC, a fault can be located only if choosing a frequency within the ghost-free bandwidth (see Fig. 1), where the pseudo-spectrum presents a single peak. In [16], it was proved that TR-MUSIC can still provide sub-millimeter resolution even when applied to such relatively low test frequencies.

At higher frequencies, ghost traces represent irreducible ambiguities in the interpretation of TR-MUSIC pseudo-spectra. This is not to say that high-frequency results have no practical use, as argued in Sec. IV. The possibility of taking advantage of results outside the ghost-free bandwidth was not acknowledged in [16], since it requires multi-frequency tests which, in case of high SNRs, present virtually no benefit with respect to the single-frequency results limited by the ghost-free bandwidth.

III. EMPIRICAL ASSESSMENT OF NOISE IMPACT ON TR-MUSIC

Theoretical analyses of the performance of MUSIC processing in presence of noise are available in the literature [24], but they apply to direction finding problems, for which MUSIC was originally introduced. While this configuration shares the same mathematical definition (1) of the pseudo-spectrum, it does not consider phenomena proper to cable networks, e.g., multiple reflections. To the best of our knowledge, there exists no theoretical framework for describing the effects of noise on MUSIC for such settings.

For this reason, an empirical approach was adopted, by using experimental data measured on two NUTs schematically represented in Fig. 2, moving from a single cable to a network structure with three branches connected through a junction. Fig. 3(a) shows the implementation of the network tested. A

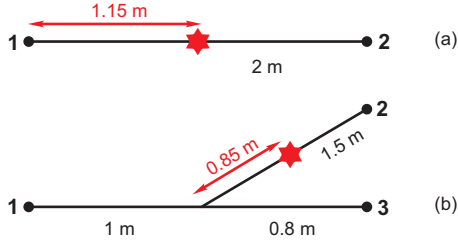


Fig. 2: Topologies of the two networks used in studying the effects of noise on locating faults with TR-MUSIC: (a) single branch and (b) single junction. The star indicates the position of the fault; each cable end, shown as black dots, was used as a testing port. Bold numbers are later used to identify the path along which TR-MUSIC location performance is evaluated.

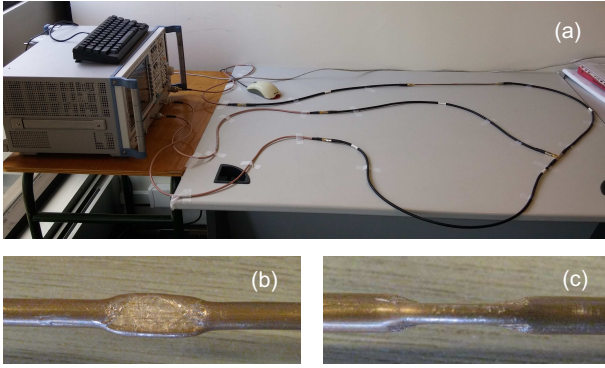


Fig. 3: The experimental setup (a) for the single-junction network, for a soft fault implemented as a crushed portion of line (b)-(c).

single soft fault was considered in both NUTs, introduced by creating a partially crushed portion about 2 cm long in a portion of semi-rigid cable, as visible in Figs. 3(b)-(c). This kind of experimental tests was successfully used in previous work; more details can be found in [16]. The scattering matrices for each tested network were measured using a Rohde & Schwarz ZVB8 vector network analyzer on a bandwidth ranging from 1 MHz to 500 MHz, sampled in 0.6 MHz steps.

The analysis of the performance of TR-MUSIC is based on the presence of an additive white Gaussian noise (AWGN), which can be thought as either representing measurement uncertainty, or alternatively reproducing the statistical behavior of signals propagating along cable networks tested while in use (on-line testing). The AWGN was numerically added to each measured scattering matrix, both for the NUT and its reference (baseline) matrix, before proceeding to the data processing stage resumed in Sec. II. The signal-to-noise ratio (SNR) was defined as the ratio of the average power scattered by the NUT (both in transmission and reflection) and the noise average power. The SNR was set to be a constant, independent from frequency, in order to simplify the comparison of the results over the entire frequency range tested.

Fig. 4 shows the local maxima detected in the pseudo-spectra obtained by applying the TR-MUSIC processing summarized in Sec. II, computed independently for each fre-

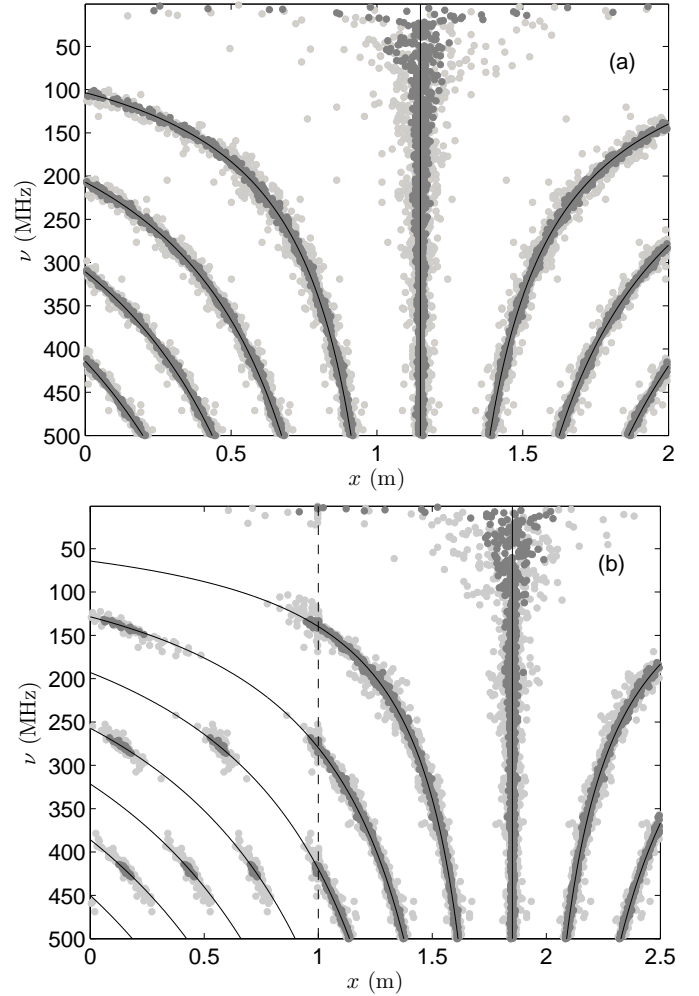


Fig. 4: Local maxima in the pseudo-spectra computed from scattering matrices measured for the two configurations in Fig. 2: (a) single-branch case and (b) single-junction case. Two noise levels are considered, a 15 dB SNR (dark gray dots) and 5 dB SNR (light gray dots), with solid black lines the theoretical results expected from (2).

quency, for two values of SNR, namely 5 and 15 dB. Reference structures for the pseudo-spectra singularities, expected under noiseless conditions, are shown as solid black lines, based on (2). Measurement-based pseudo-spectra (dots) in Fig. 4 show how noise affects TR-MUSIC, by inducing a stochastic dispersion in the pseudo-spectra peaks, with the original positions $p_n(\nu)$ of the traces (black lines) perturbed into estimates $\hat{p}_n(\nu)$. The errors in these estimates exceed the millimeter spatial resolution demonstrated in [16], undercutting the benefits of this super-resolution method.

Results for the single-junction network in Fig. 4 (bottom graph) cover the results for positions along the two branches connected ending into ports (1) and (2) in Fig. 2. They are therefore interesting since they show how TR-MUSIC identifies the branch containing the fault, with the ghost traces abruptly stopping at the junction (1 m). Some peaks are still visible between 0 and 1 m, again due to periodicity in the

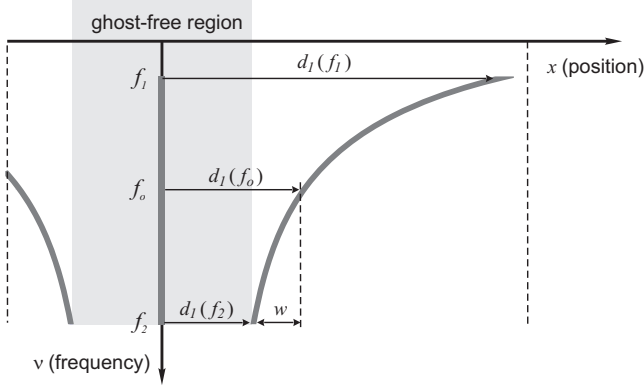


Fig. 5: Bin design for maximum contrast in pseudo spectra-based histograms.

Green functions, but exist only at those frequencies where ghost traces intersect the end of the cable, here at 1 m: peaks are then observed only at distances that need to be a multiple of half the wavelength at these frequencies.

The dispersion caused by noise in the pseudo-spectrum structure appears to be inversely dependent on the frequency, with the ghost-free bandwidth¹, at the lower frequency end, more prone to disruption. The sub-millimeter resolution observed in [16] for a noiseless case gives way to a statistical dispersion that can exceed one meter below 10 MHz for a 5 dB SNR. On the contrary, much lower dispersions are observed at higher frequencies: the reason for this frequency-dependent behavior can be traced back to the fact that the spatial scale of the pseudo-spectrum fundamentally responds according to the wavelength associated to each frequency.

In order not to lose the super-resolved location property, TR-MUSIC should therefore be applied to higher frequencies in case of noisy data, eventually moving outside the ghost-free bandwidth. The problem with such a proposal is: TR-MUSIC treats each frequency data independently, and is therefore unable to provide unambiguous estimates of the fault position, since for each frequency outside the ghost-free bandwidth, TR-MUSIC results into a set of multiple peaks $\{\hat{p}_n(\nu)\}$ of which only $\hat{p}_0(\nu)$ is a meaningful estimate of the fault location. A solution to this problem is discussed in Sec. IV, based on sets of data obtained at multiple frequencies, together with guidelines for designing a robust multiple-frequency TR-MUSIC processing.

IV. MULTI-FREQUENCY LOCATION ESTIMATOR

The results discussed in the previous section highlighted the need to control the statistical dispersion introduced by noise, in order to counter the effects of noise and avoid wasting the potential for super-resolved location. One way of doing this is to use average-based estimators, by looking at the positions yielded by TR-MUSIC pseudo-spectrum collectively, as populations of random samples sharing a common information, i.e.,

the fault position. To this end, the following meta-estimator is introduced

$$\hat{p} = \frac{1}{N_F} \sum_{k=1}^{N_F} \hat{p}_0(f_k), \quad (3)$$

based on the results of N_F frequencies $\{f_k\}$ and the individual fault-position estimates $\{\hat{p}_0(f_k)\}$ yielded by single-frequency TR-MUSIC processing discussed in Secs. II and III. In the following, it will be assumed that the N_F frequencies are used during TR-MUSIC tests, uniformly distributed between frequency f_1 and f_2 , with a sampling step Δf .

In order to apply (3), two problems need to be addressed: a) to automatically identify and isolate the estimates $\{\hat{p}_0(f_k)\}$ belonging to the fault trace; b) to know how (3) performs, depending on which, and how many, frequencies are tested.

One way of identifying the fault trace is to notice that the number of occurrences of peaks in the pseudo-spectrum is maximized when observing the positions x close to the fault, because of the expected frequency-invariance of the fault trace (see Figs. 1 and 4). Elsewhere, contributions from ghost traces would otherwise be spread over wider intervals, thus resulting in a lower frequency of occurrence. An empirical probability of identifying the fault trace can be obtained by subdividing an NUT into short sections of length w , or bins, and counting the occurrences of estimates $\hat{p}_n(\nu)$ obtained from TR-MUSIC, effectively producing an histogram. Examples are later shown in Fig. 6.

With reference to Fig. 5, the bin width w should be chosen in such a way as to capture the maximum number of samples belonging to the fault trace, thus requiring a larger w , while at the same time minimizing the probability of including samples from neighboring ghost traces, hence requiring a narrower bin. The former requirement cannot be met at the same time for low and high frequencies, because of the frequency-dependent statistical dispersion, while the latter can be satisfied by setting

$$w = \alpha d_1(f_2), \quad (4)$$

with $\alpha \in [0, 1]$ a scaling factor. The minimum distance $d_1(f_2)$ between a ghost and the fault trace is used as a reference, and it also defines the ghost-free region shown in Fig. 1. For larger values of w the bin would capture both fault- and ghost-trace samples.

The relative positions of bins and the fault will not be known at this time, so that the worst case is considered in Fig. 5, where one of the bins has one of its edges in close proximity of a first-order ghost trace: here, the ghost trace has maximum slope, and will thus result in a smaller footprint over the horizontal axis, thus yielding a maximum density of occurrences of estimates $\hat{p}_1(f_k)$; higher-order ghost traces will result in a lower density of occurrences. The number N_g of occurrences for this bin can be computed by first finding the frequency f_o associated to the right edge of the bin, such that $d_1(f_2) + w = d_1(f_o)$, hence

$$f_o = \frac{f_2}{1 + \alpha}, \quad (5)$$

from which

$$N_g = \frac{f_2 - f_o}{\Delta f} = \frac{f_2}{\Delta f} \frac{\alpha}{1 + \alpha}, \quad (6)$$

¹< 100 MHz for the single cable and < 125 MHz for the network

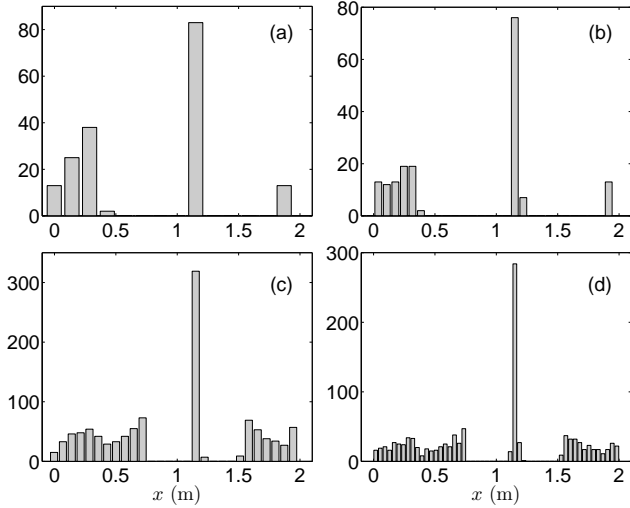


Fig. 6: Number of peaks per bin for the results in Fig. 4(a), for the single-cable case and a 15 dB SNR. The four histograms correspond to $1/\alpha = 5.5$ and 10.5 (left and right columns), for data collected on the frequency ranges 100-150 MHz and 100-300 MHz (top and bottom rows).

to be compared with the N_F occurrences ideally observed for another bin over the fault trace. The identification of the fault region is therefore possible only if $N_F/N_g \geq M$, with $M > 1$ the contrast required between the background and the peak of the histogram. Recalling that $N_F = (f_2 - f_1)/\Delta f$, the contrast reads

$$N/N_g = (1 - f_1/f_2) \frac{\alpha}{1 + \alpha}, \quad (7)$$

and will be larger than M if

$$\alpha \leq \left(\frac{M}{1 - f_1/f_2} - 1 \right)^{-1}. \quad (8)$$

In this simple deterministic model, the number N_F of tested frequencies has no effect on the ability to identify the fault region from a pseudo-spectrum, which is rather controlled by the bandwidth spanned by the test frequencies. As an example, for $M = 2$ and $f_2/f_1 = 1.5$, $\alpha < 1/6$; for higher contrasts, the bins will have to be a smaller fraction of the ghost-free region.

Fig. 6 presents a few examples of histograms obtained with different choices of w and f_2/f_1 . One bin stands out in each histogram, and corresponds to the fault trace. The average of the samples $\{\hat{p}_0(f_k)\}$ falling into this bin can be used as an initial guess \hat{p} of the fault position. From this point onwards, it is possible to redistribute the bins in order to ensure that one of them will be centered on \hat{d}_0 , thus reducing the probability of having the fault-trace sample population divided over two adjacent bins, which would otherwise result into a lower contrast M . Fig. 6 correspond to the case of a bin already centered on the fault position.

The population of single-frequency estimators $\{\hat{p}_0(f_k)\}$ needed in order to compute the meta-estimator (3) is selected by extracting those peak positions in the pseudo spectrum that fall in the region $\hat{p} \pm d_1(f_2)/2$, which sits halfway between

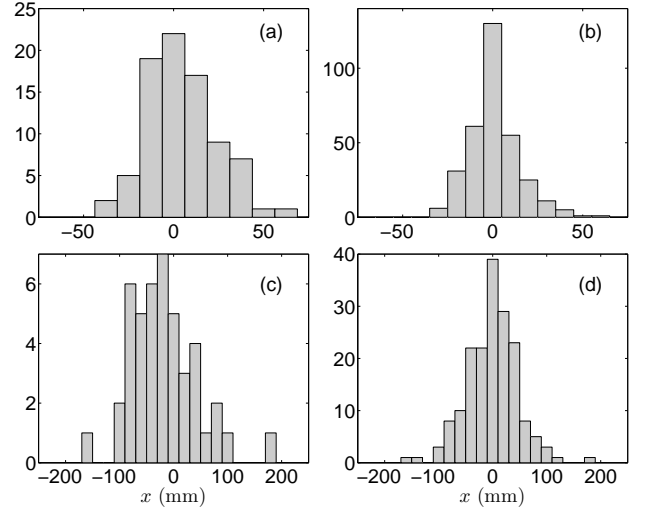


Fig. 7: Empirical probability density function of fault-trace estimates \hat{p}_0 extracted from data for 100-150 MHz (left) and 100-300 MHz (right) for the single-cable case, for a 15 dB SNR (top) and 5 dB (bottom).

the fault trace and the left and right first-order ghost traces. The population thus isolated does not correspond exactly to the entire set of fault-trace samples $\{\hat{p}_0(f_k)\}$, but will only capture samples falling within the ghost-free region (cf. Fig. 5). Fig. 7 shows the distribution of these samples around the actual fault position.

The precision of the meta-estimator (3) can be estimated by modeling the N_F estimates $\{\hat{p}_0(f_k)\}$ as zero-average independent Gaussian random variables, approximating their standard deviation σ as

$$\sigma(\nu) = \sigma_o/\nu, \quad (9)$$

for which the variance of \hat{p} would be

$$\begin{aligned} \sigma_{\hat{p}}^2 &= \frac{1}{N_F^2} \sum_{n=1}^{N_F} \sigma^2(f_n) = \frac{\sigma_o^2}{\Delta f^2 N_F^2} \sum_{q=n_1}^{n_2} q^{-2} \simeq \\ &\simeq \frac{\sigma_o^2}{\Delta f^2 N_F^2} \int_{n_1}^{n_2} dq q^{-2} = \frac{\sigma_o^2}{N_F f_1 f_2}, \end{aligned} \quad (10)$$

which is equivalent to the variance of a population of N_F i.i.d. samples measured at the frequency $f_c = \sqrt{f_1 f_2}$.

It is worth recalling that the requirement of sweeping the bandwidth $[f_1, f_2]$ was driven by the need to isolate a population of coherent estimates of the fault position apart from ghost traces, and that the accuracy of the TR-MUSIC estimators improves with the frequency. Eq. (10) explains the trade-off between the increased number of samples associated to a larger bandwidth and the fact that those at the higher end will outperform those obtained at lower frequency, as made clear by Fig. 4. In other words, low-frequency samples contribute mostly to the identification of the fault trace, but limit the overall accuracy of the estimator \hat{p} , which cannot reach the accuracy expected for high-frequency samples.

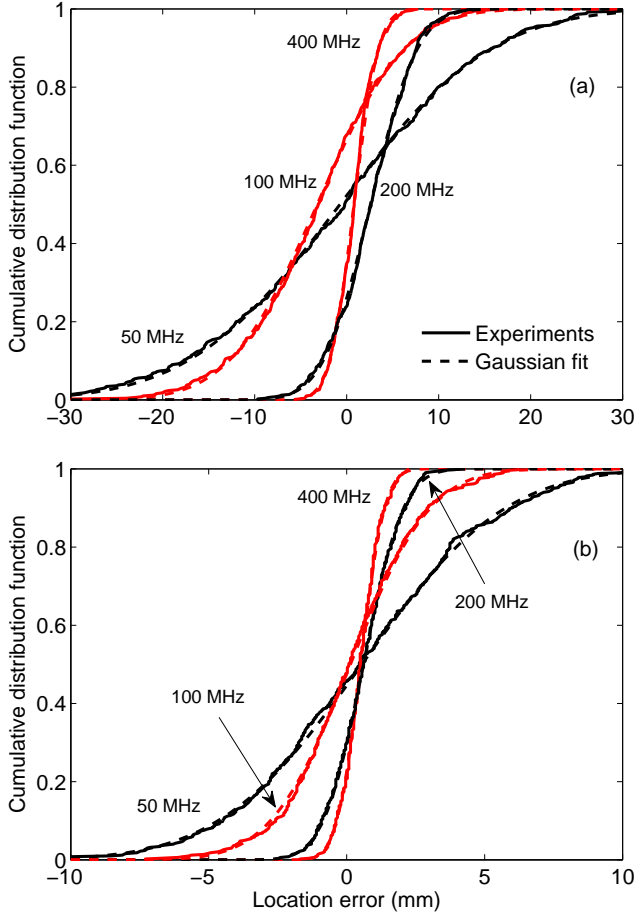


Fig. 8: Empirical distribution functions estimated from 500 random realizations of the multi-frequency estimator computed from experimental results for a single-branch configuration, for a 50 MHz bandwidth, with minimum frequencies shown near each set of curves, for an SNR equal to: (a) 5 dB and (b) 15 dB.

The minimum bandwidth required in order to identify the fault trace is found as a corollary of (7)

$$f_2/f_1 \geq \left(1 - \frac{M\alpha}{1+\alpha}\right)^{-1}, \quad (11)$$

in order to ensure a given contrast M in the histograms in Fig. 6 and thus the identification of the fault trace. Notice that (11) is valid under the condition $M\alpha/(1+\alpha) < 1$. This deterministic model can be accurate only if $w > 2\sigma(\nu)^2$, $\forall \nu \in [f_1, f_2]$, with f_1 yielding the worst case, thus

$$\alpha > 4 \frac{\sigma_o f_2}{v f_1}, \quad (12)$$

based on (4) and (9).

Therefore, small fractional bandwidths f_2/f_1 are an unlikely option for either very low SNR or at low frequencies, where $\sigma(\nu)$ might prove to be too large.

²i.e., for a 95 % confidence interval

V. ACCURACY OF THE MULTI-FREQUENCY ESTIMATOR

The precision of the proposed estimator, as predicted by (10), was verified by generating 500 random realizations of additive noise. Associated populations of single-frequency estimators were derived, by first computing the pseudo spectra for the two cable configurations in Fig. 2, covering the frequencies from 1 to 500 MHz.

The multi-frequency estimator \hat{p} in (3) can be expected to approximately follow a Gaussian probability distribution, since it is based on the summation of random quantities, namely the fault-trace positions $\{\hat{p}_0(f_k)\}$. Therefore, only the first two moments of \hat{p} need to be studied, providing a direct assessment of the presence of a bias in \hat{p} and its precision, following its standard deviation. The validity of this choice is demonstrated in Fig. 8, where the empirical distribution function of \hat{p} is shown for results obtained for the single-branch case, with a 5 and 15 dB SNR, for a fixed frequency band equal to 50 MHz and a starting frequency f_1 moving from 50 up to 400 MHz. Gaussian distributions were fitted to the empirical ones, resulting in a close agreement spanning at least two standard deviations, i.e., for at least 95 % of the cases.

The average error $\hat{p} - p$ and the standard deviation of \hat{p} are shown in Figs. 9 and 10 for the two test configurations in Fig. 2, for a 15 dB SNR. Data were computed over two bandwidths, namely 25 and 50 MHz, with the starting frequency f_1 moving from 50 up to 400 MHz.

All sets of results present a residual bias way smaller than the standard deviation, indicating an unbiased estimator, with typical values below 1 mm even for $f_1 = 50$ MHz. Therefore the precision is limited by the standard deviation of the estimator (3). The standard deviation decreases with f_1 , while the number of frequency samples is kept constant, i.e., the same number of single-frequency estimates $\{\hat{p}_0(f_k)\}$ are used. Therefore, the fact that $\sigma_{\hat{p}}$ decreases with f_1 is explained by the decreasing dispersion of $\{\hat{p}_0(\nu)\}$ at higher frequency, as postulated in (9), rather than because of the averaging in (3). The transition between results in the ghost-free region (50-100 MHz) and those at higher frequency is noteworthy, confirming the effectiveness of the proposed data processing.

Comparisons of empirical results with (10) are presented, obtained by estimating σ_o by means of a least-square procedure; in practical settings, (10) provides the means for estimating σ_o from preliminary tests for a single configuration $[f_1, f_2]$. The results in Figs. 9 and 10 confirm that (10) can explain how choosing different test bandwidths $[f_1, f_2]$ impacts the accuracy of the multi-frequency estimator; this also indirectly confirms the validity of (9) as a working approximation. Therefore, (10) can be used in order to predict how the precision of the proposed estimator would change by passing from a test carried out over a frequency range $[f_1, f_2]$ for N_F frequency samples, to another with $[f'_1, f'_2]$ with N'_F samples. The standard deviation is expected to be reduced by a factor

$$\sqrt{\frac{N'_F f'_1 f'_2}{N_F f_1 f_2}}. \quad (13)$$

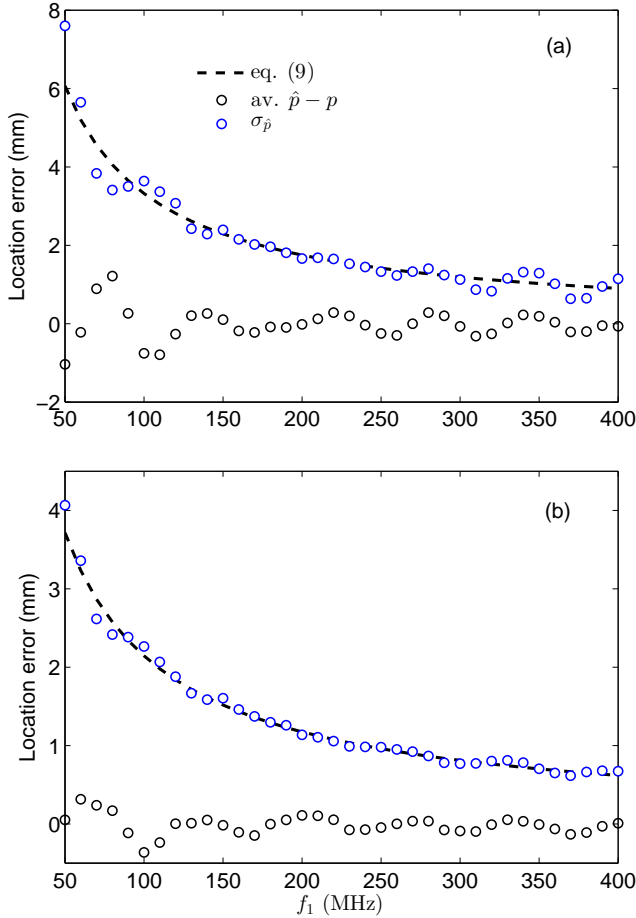


Fig. 9: Average location error and its standard deviation for the multi-frequency estimator (3) for the single-cable case for a 15 dB SNR, for a (a) 25 MHz and (b) 50 MHz bandwidth. $\sigma_o = 2.4 \times 10^6$ m/s was estimated from these results.

With a standard deviation below 8 mm at $f_1 = 50$ MHz, for a 25 MHz bandwidth, these results confirm that super-resolved location of faults is still possible even with data affected by noise. In fact, at this frequency the wavelength is expected to be about 5 m in PTFE-based coaxial cables, and for a bandwidth of 25 MHz, time-domain test signals could not be shorter than about 40 ns, with a spatial footprint around 9 m.

The performance of (3) *versus* the SNR is presented in Fig. 11, for an SNR going from 5 to 30 dB and a 50 MHz bandwidth, starting at 50 and 200 MHz. These results prove that even at very low SNR levels TR-MUSIC can be expected to locate faults with high resolution; e.g., at 5 dB SNR, the fault is identified with a standard deviation of about 25 mm, using data measured on a [50 – 100] MHz bandwidth. The standard deviation observed for the [200 – 250] MHz data is expected to be about $\sqrt{10} \simeq 3.2$ lower than the one found for [50 – 100] MHz data, according to (13), a prediction confirmed accurate to better than 12 % in Fig. 11.

VI. CONCLUSION

This paper has investigated the performance of TR-MUSIC in the presence of noise. In spite of its high resolution, noise

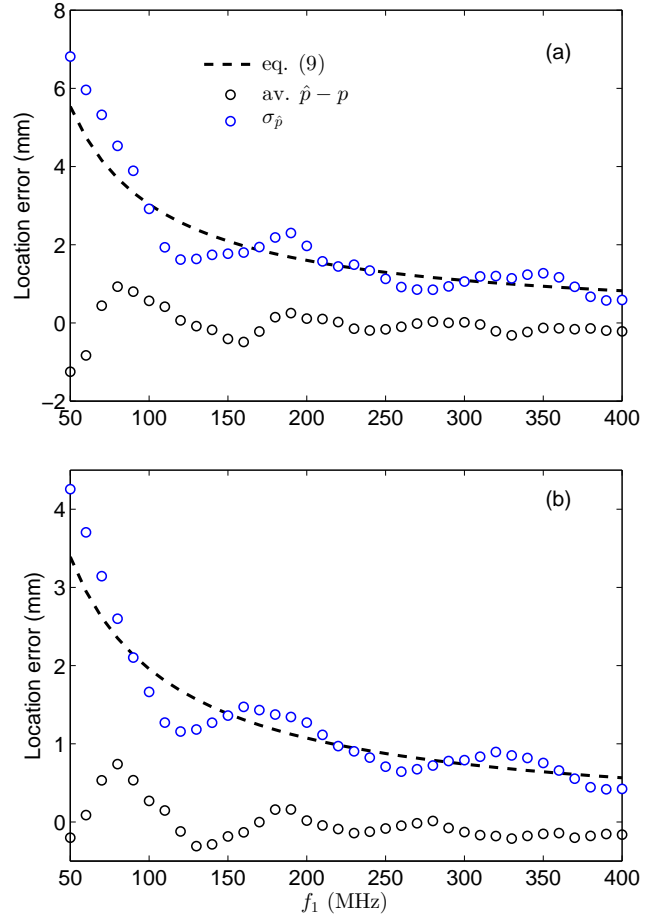


Fig. 10: Same as in Fig. (9), but for the single-junction case. $\sigma_o = 2.2 \times 10^6$ m/s was estimated from these results.

leads to stochastic dispersion, especially at the low frequencies for which the method was first proposed for locating soft faults. The opportunity of exploiting the lower dispersion reported at higher frequencies is hindered by the appearance of spurious locations, or ghost traces, from which the actual fault position cannot be directly inferred.

An alternative multi-frequency estimator, based on independent single-frequency results, was introduced, in order to counter the loss of accuracy. The majority-based rule introduced in order to isolate meaningful estimates of the fault position is shown to be effective. Formal tools were introduced in order to design robust estimators even though working within the ghost region. The results presented confirm the accuracy of these tools and the feasibility of preserving a super-resolved location of soft faults even with SNR levels as low as 5 dB.

These results require an accurate description and modeling of a network under test, in order to compute its Green functions, which are needed in TR-MUSIC processing. Future work will analyze how errors in the computation of the Green functions, e.g., because of an inaccurate description, would impact the accuracy of TR-MUSIC in locating faults.

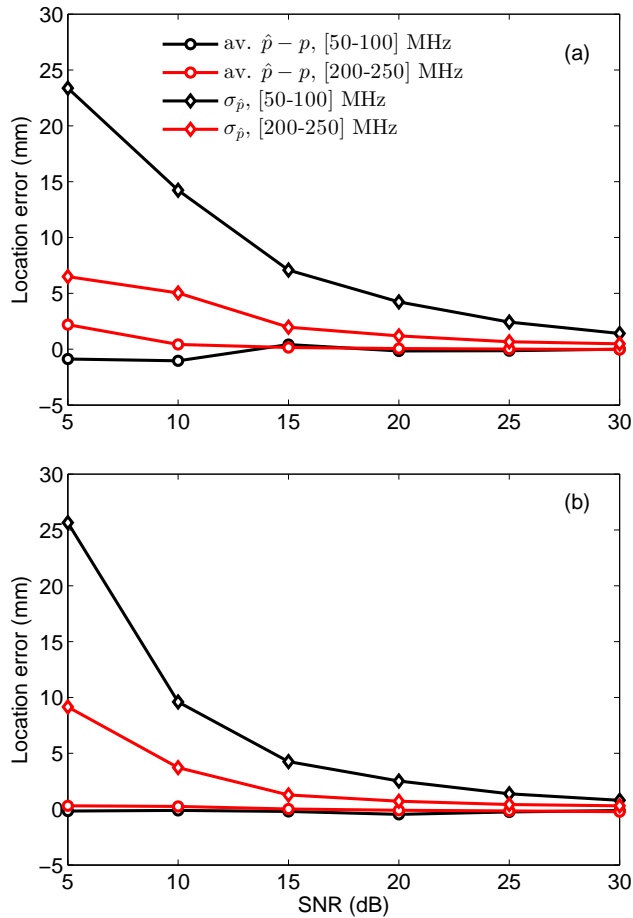


Fig. 11: Performance of the multi-frequency estimator (3) versus SNR in locating a fault, for the two systems in Fig. 2, respectively.

REFERENCES

- [1] C. Furse and R. Haupt, "Down to the wire," *Spectrum, IEEE*, vol. 38, no. 2, pp. 34–39, February 2001.
- [2] C. Furse, Y. C. Chung, R. Dangol, M. Nielsen, G. Mabey, and R. Woodward, "Frequency-domain reflectometry for on-board testing of aging aircraft wiring," *Electromagnetic Compatibility, IEEE Transactions on*, vol. 45, no. 2, pp. 306–315, May 2003.
- [3] C. Buccella, M. Feliziani, and G. Manzi, "Detection and localization of defects in shielded cables by time-domain measurements with UWB pulse injection and clean algorithm postprocessing," *IEEE Trans. Electromagn. Compat.*, vol. 46, no. 4, pp. 597–605, November 2004.
- [4] P. Smith, C. Furse, and J. Gunther, "Analysis of spread spectrum time domain reflectometry for wire fault location," *IEEE Sensors Journal*, vol. 5, no. 6, pp. 1469–1478, December 2005.
- [5] C. Furse, Y. C. Chung, C. Lo, and P. Pendayala, "A critical comparison of reflectometry methods for location of wiring faults," *Smart Structures and Systems*, vol. 2, no. 1, pp. 25–46, 2006.
- [6] S. Schuet, D. Timucin, and K. Wheeler, "A model-based probabilistic inversion framework for characterizing wire fault detection using TDR," *IEEE Trans. Instrum. Meas.*, vol. 60, no. 5, pp. 1654–1663, May 2011.
- [7] A. Cozza, "Never trust a cable bearing echoes: Understanding ambiguities in time-domain reflectometry applied to soft faults in cables," *IEEE Trans. Electromagn. Compat.*, to be published.
- [8] B. M. Oliver, "Time domain reflectometry," *Hewlett-Packard Journal*, vol. 15, no. 6, pp. 1–7, 1964.
- [9] E. Song, Y.-J. Shin, P. Stone, J. Wang, T.-S. Choe, J.-G. Yook, and J. B. Park, "Detection and location of multiple wiring faults via time-frequency-domain reflectometry," *IEEE Trans. Electromagn. Compat.*, vol. 51, no. 1, pp. 131–138, February 2009.
- [10] C. K. Lee, K. S. Kwak, T. S. Yoon, and J. B. Park, "Cable fault localization using instantaneous frequency estimation in gaussian-enveloped linear chirp reflectometry," *IEEE Trans. Instrum. Meas.*, vol. 62, no. 1, pp. 129–139, January 2013.
- [11] S. J. Chang and J. B. Park, "Multiple chirp reflectometry for determination of fault direction and localization in live branched network cables," *IEEE Trans. Instrum. Meas.*, vol. 66, no. 10, pp. 2606–2614, October 2017.
- [12] J. Zhang, Y. Zhang, and Y. Guan, "Analysis of time-domain reflectometry combined with wavelet transform for fault detection in aircraft shielded cables," *IEEE Sensors Journal*, vol. 16, no. 11, pp. 4579–4586, June 2016.
- [13] Y. J. Shin, E. J. Powers, T. S. Choe, C.-Y. Hong, E.-S. Song, J.-G. Yook, and J. B. Park, "Application of time-frequency domain reflectometry for detection and localization of a fault on a coaxial cable," *IEEE Trans. Instrum. Meas.*, vol. 54, no. 6, pp. 2493–2500, December 2005.
- [14] S. Naik, C. M. Furse, and B. Farhang-Boroujeny, "Multicarrier reflectometry," *IEEE Sensors Journal*, vol. 6, no. 3, pp. 812–818, June 2006.
- [15] F. Auzanneau, "Wire troubleshooting and diagnosis: Review and perspectives," *Progress In Electromagnetics Research B*, vol. 49, pp. 253–279, 2013.
- [16] M. Kafal, A. Cozza, and L. Pichon, "Locating faults with high resolution using single-frequency TR-music processing," *IEEE Trans. Electromagn. Compat.*, vol. 65, no. 10, pp. 2342–2348, October 2016.
- [17] F. K. Gruber, E. A. Marengo, and A. J. Devaney, "Time-reversal imaging with multiple signal classification considering multiple scattering between the targets," *The Journal of the Acoustical Society of America*, vol. 115, no. 6, pp. 3042–3047, 2004.
- [18] M. Fleming, M. Lowe, F. Simonetti, and P. Cawley, "Super resolution imaging: performance studies," in *AIP Conference Proceedings*, vol. 820, no. 1. AIP, 2006, pp. 736–743.
- [19] M. Davy, J.-G. Minonzio, J. de Rosny, C. Prada, and M. Fink, "Influence of noise on subwavelength imaging of two close scatterers using time reversal method: Theory and experiments," *Progress In Electromagnetics Research*, vol. 98, pp. 333–358, 2009.
- [20] L. A. Griffiths, R. Parakh, C. Furse, and B. Baker, "The invisible fray: A critical analysis of the use of reflectometry for fray location," *IEEE Sensors Journal*, vol. 6, no. 3, pp. 697–706, June 2006.
- [21] G. Cerri, R. De Leo, L. Della Nebbia, S. Pennesi, V. M. Primiani, and P. Russo, "Fault location on shielded cables: Electromagnetic modelling and improved measurement data processing," *IEE Proceedings - Science, Measurement and Technology*, vol. 152, no. 5, pp. 217–226, September 2005.
- [22] L. Abboud, A. Cozza, and L. Pichon, "A noniterative method for locating soft faults in complex wire networks," *IEEE Trans. Veh. Technol.*, vol. 62, no. 3, pp. 1010–1019, March 2013.
- [23] R. O. Schmidt, "Multiple emitter location and signal parameter estimation," *IEEE Trans. Antennas Propag.*, vol. 34, no. 3, pp. 276–280, March 1986.
- [24] P. Stoica and A. Nehorai, "MUSIC, maximum likelihood, and Cramer-Rao bound," *IEEE Trans. Acoust., Speech, Signal Process.*, vol. 37, no. 5, pp. 720–741, May 1989.